sciendo

Two novel potent perfluorophenylhydrazone derivatives, 1-((4-bromothiophen-2-yl)methylene)-2-(perfluorophenyl) hydrazine, and 1-((4-bromo-5-methylthiophen-2-yl)methylene)-2-(perfluorophenyl)hydrazine as multi-target compounds to combat Alzheimer disease and their crystal, molecular, and electronic properties

Július Sivý[1], Dušan Bortňák[2], Daniel Végh[2], Erik Rakovský[3]

[1]*Faculty of Mechanical Engineering, STU, Námestie slobody 17, Bratislava 1, SVK-812 31, Slovak Republic*
[2]*Institute of Organic Chemistry, Catalysis and Petrochemistry, Faculty of Chemical and Food Technology, STU, Radlinského 9, Bratislava 1, SVK-812 37, Slovak Republic*
[3]*Department of Inorganic Chemistry, Faculty of Natural Sciences, Comenius University, Ilkovičova 6, Bratislava 4, SVK-842 15, Slovak Republic*
julius.sivy@stuba.sk

Abstract: Two potent novel perfluorophenylhydrazone derivatives are presented as multi-target compounds to combat Alzheimer disease $C_{11}H_4BrF_5N_2S$, 1-((4-bromothiophen-2-yl)methylene)-2-(perfluorophenyl) hydrazine, (**I**) and $C_{12}H_6BrF_5N_2S$, 1-((4-bromo-5-methylthiophen-2-yl)methylene)-2-(perfluorophenyl) hydrazine, (**II**), which can potentially be improved by further design. Their multi-target structures and features have been combined as potential AD therapeutics. Crystals (**I**), and (**II**), are molecules with two rings and a hydrazone part as a centre of the molecule. The compounds have been synthesised and characterised by elemental spectroscopic (^{1}H-NMR) analysis. Crystal structures of the solid phase were determined by single crystal X-ray diffraction method. Both compounds crystallise in the monoclinic space group with $Z = 4$ and $Z = 2$ molecules per unit-cell. Compound (**I**) crystallises as a racemate in the centrosymmetric space group and compound (**II**) crystallises as a non-racemate in the non-centrosymmetric space group. Their "absolute configuration and conformation for bond values" were derived from the anomalous dispersion (rmad) for (**II**). Crystal structures revealed diverse non-covalent interactions such as intra- and inter-hydrogen bonding, π-ring$\cdots\pi$-ring, C—H$\cdots\pi$-ring. The expected stereochemistry of hydrazones atoms C7, N2 and N1 were confirmed for (**I**) and (**II**). Both molecules show "boat conformation" like a 6-membered ring. Results of single crystal studies were reproduced with the help of Hirshfeld surface study and Gaussian software.

Keywords: *Ab initio* DFT/B3LYP/6-311G/Auto calculation, hydrazine, Hirshfeld surface, hydrogen interactions, single-crystal X-ray study

Introduction

Microbial resistance to antibiotics is an urgent and well-known problem worldwide. Several hydrazones synthesised under benign reaction conditions have proved to be potent growth inhibitors of drug-resistant strains of *Staphylococcus aureus* and *Acinetobacter baumannii* with minimum inhibitory concentration values. These molecules are non-toxic to human cells at appropriate concentrations. Although hydrazones possess greater intrinsic hydrolytic stability than the corresponding imines, these molecules can be converted into the starting materials by reacting with water under physiological condition. Antimicrobial activity of hydrazones is probably caused by the hydrolysed products, aldehydes, and hydrazines. For example, the aldehyde derivative did not show any activity, but the hydrazine showed weak growth inhibition. Thus, it can be concluded that the antimicrobial activity of the compounds is due to their hydrazone functional groups, not due to their possible hydrolysed products. Fluorine substitution has been extensively studied in drug discovery to enhance biological activity and increase chemical and metabolic stability of the resultant molecules. Hydrazone derivatives have been designed and synthesised not only for antimicrobial studies. They are of general wide interest not only in medicinal chemistry (Verma et al., 2014; Kuman and Chauhan, 2014; Giliberti et al., 2010; Bari et al., 2019; Tonelli et al., 2008; Saha et al., 2019) but also in material chemistry (Su and Aprahamian, 2014; Burdette, 2012; Feringa and Browne, 2011; Xu et al., 2018; Lukeš et al. 2016; Sandoval-Torrientes et al., 2017; Beverina et al., 2011; Tarabová and Milata, 2012), and they

exhibit nematicidal and insecticidal activity (Eloh et al., 2015). Hydrazones exhibit a broad spectrum of biological activities and have been described in the treatment of tuberculosis, malaria, and cancer. They have also been identified as strong radical scavengers and their multitarget properties have been combined as potential Alzheimer's disease (AD) therapeutics. Hydrazones were found to be very good inhibitors of amyloid beta fibril and oligomer formation and they showed highly effective radical scavenging properties (Baier et al., 2021). N-pentafluorophenyl substituted hydrazones can also be used as analytical reagents. Two principles are most often used in the analysis:

1. Interaction of an ion (anion, cation) with a secondary amino group leading to a colour change after the addition of the analyte.
2. Formation of a stable molecular ion or a fragment well detectable in mass spectrometry (usually pentafluorophenyl).

Ions such as the fluoride anion (Ghosh et al., 2018; Chowdhury et al., 2015) (Scheme 1, 2, 3) can be well determined. Fluorine is the thirteenth most abundant element on Earth and occurs mainly in form of the minerals fluorite, fluorapatite, and cryolite. Only twelve organic compounds of fluorine have been identified in nature, all of which show considerable toxicity. Despite the low occurrence of fluoroorganic compounds in nature, which are without exception highly toxic, chemical research and industry currently produce thousands of new fluorine-containing organic compounds. The year 1941 is considered the beginning of synthetic fluoroorganic chemistry. According to data from the Internet, global demand for fluorine-containing chemicals in 2015 reached 3.35 million tons per year. Due to the wide range of issues in different research works, crystal, molecular and electronic properties of N-pentafluorophenyl hydrazones will be discussed. These compounds show diverse crystal-molecular interactions including interactions such as $\pi\cdots\pi$, C—H$\cdots\pi$, etc. Here, the crystal-base structural properties were investigated by the single crystal X-ray diffraction method, Gaussian method, and the Hirshfeld surface analysis. Synthesis, molecular, crystal, and electronic structure of title compounds (**I**) and (**II**) are reported. The interest of our research group is to develop novel hydrazone derivative routes for their synthesis in simple and efficient ways. Molecules of the title compounds crystallise in the space group $P2_1/n$ and *Pn*. Accordingly, compound (**I**) is a racemate and consists of one molecule in the independent part of the unit-cell with relative configuration of carbon atoms, while compound (**II**) is a non-racemate and consists of one molecule in the independent part of the unit-cell. Hydrazone part of the molecule and its left and right side possess "a boat conformation" like a 6-membered ring. The first right-side ring, hexafluorophenyl, is planar and adopts a plane conformation, while atom N1 is displaced from this plane with the out-of-plane displacement of 0.011 (3) for (**I**) and 0.034 (7) Å for (**II**); out-of-plane displacement for atoms F1, F2, F3, F4, F5 is 0.078 (3), –0.039 (3), –0.013 (3), 0.018 (3), –0.028 (3) for (**I**), and 0.075 (7), –0.032 (8), 0.009 (7), –0.009 (7), –0.047 (6) Å, (**II**). The second left-side ring, thiophene, is also planar, the out-of-plane displacement for atom Br1 is –0.013 (3) for (**I**) and –0.008 (7), (**II**) and for atom C12 it is 0.066 (10) Å, (**II**).

Dihedral angle between the planes is 32.00 (5)° for (**I**) and 31.77 (11)° for (**II**). Compounds (**I**) and (**II**) were investigated by *ab initio* DFT/B3LYP/6-311G calculations, and properties of the conformation of products (**I**) and (**II**) were checked by X-ray structure determination. Title compound (**I**) (Scheme 1) as a hydrazone derivative crystallises in the centrosymmetric space group, while title compound (**II**) (Scheme 2) as a hydrazone derivative crystallises in the non-centrosymmetric space group (monoclinic crystal system). Simple Hirshfeld surface analysis was used to visualize the map for the different intermolecular interactions (energies) in the crystal structure and the Gaussian natural bond order analysis was performed (Frisch et al., 2016).

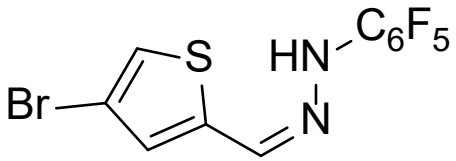

Scheme 1. Molecular scheme of title compound (**I**).

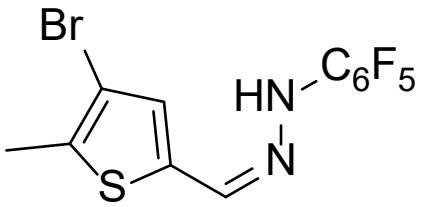

Scheme 2. Molecular scheme of title compound (**II**).

Material and Methods

Chemicals

Synthesis and crystallisation

Compounds (**I**) and (**II**) were prepared according to a standard protocol (Scheme 3) described in literature. All NMR spectra were obtained using an INOVA NMR 300 MHz spectrometer (operating fre-

quencies 300 MHz (^{1}H), 75 MHz (^{13}C), and 282 MHz (^{19}F)) equipped with an inverse triple resonance probe and a standard tuneable X/H probe with the possibility to tune the high frequency channel to the resonance frequency of ^{19}F. Tetramethylsilane was used to calculate the ^{1}H and ^{13}C chemical shift scales and for correct reference using the (residual) solvent signals (2.50 and 39.52 ppm for DMSO, and 7.26 and 77.00 ppm for chloroform). $CFCl_3$ was used to calculate the ^{19}F chemical shift scale; in order to correctly reference the ^{19}F chemical shift scale, an automatic referencing mechanism exploiting the ^{2}H signal of the deuterated solvent was used.

General procedure for hydrazone synthesis

To a solution of the corresponding aldehyde in 20 ml of ethanol, ethanolic solution (10 ml) of pentafluorophenylhydrazine was added. Then, a catalytic amount of concentrated hydrochloric acid was added (approximately 3—5 drops) and the reaction mixture was refluxed for 8 hours (under TLC + UV control). The solvent was evaporated under reduced pressure and the residue was crystallised from ethanol to obtain pentafluorophenylhydrazone (**I**) — (**II**).

1-((4-Bromothiophen-2-yl)methylene)-2-(perfluorophenyl) hydrazine, (I), (Scheme 3)

4-Bromothiophene-2-carbaldehyde (1.000 g, 5.23 mmol, 1 eq.) and pentafluorophenylhydrazine (1.037 g, 5.23 mmol, 1 eq.) were left to react in ethanol following the general procedure for hydrazones synthesis. Hydrazone (**I**) was obtained as a brown crystalline matter in a 51 % yield (0.991 g), m.p. 138—140 °C. ^{1}H NMR (300 MHz): δH = 7.07 (d, J = 1.3 Hz , ^{1}H), 7.20 (d , J = 1.1 Hz, ^{1}H), 7.88 (s, ^{1}H). ^{13}C NMR (75 MHz): δC = 109.88, 119.75, 124.26, 129.87 135.78, 136.05, 138.15, 139.67. ^{19}F NMR (282 MHz): δF = –165.80 (tt, J = 3.8 Hz, J = 21.6, ^{1}F), –163.30 (dt, J = 4.8 Hz, J = 21.4, ^{2}F), –155.64 (d, J = 21.6, ^{2}F).

1-((4-Bromo-5-methylthiophen-2-yl)methylene)-2-(perfluorophenyl)hydrazine, (II) (Scheme 3)

4-Bromo-5-methylthiophene-2-carbaldehyde (1.000 g, 4.88 mmol, 1 eq.) and pentafluorophenylhydrazine (0.966 g, 4.88 mmol, 1 eq.) were left to react in ethanol following the general procedure for hydrazones synthesis. Hydrazone (**II**) was obtained as a brown crystalline matter in a 60 % yield (1.127 g), m.p. 153—155 °C. ^{1}H NMR (300 MHz) δ 10.37 (s, ^{1}H), 8.17 (s, ^{1}H), 7.23 (s, ^{1}H), 2.34 (s, ^{3}H). ^{13}C NMR (75 MHz) δ 137.7 (dm J = 245 Hz), 137.3 (dm J = 246 Hz) 137.2, 136.0, 135.0, 133,9 (dm J = 247 Hz) 129.9, 120.8 (m) 108.7, 14.6. ^{19}F NMR (282 MHz): δF= –169.73 (m, ^{1}F), –164.33 (m, ^{2}F), –155.75 (m, ^{2}F) (Bortňák et al., 2020).

Crystallography and Hirshfeld surface analysis

Manuals: "The CIF file, refinement details and validation of the structure, IUCr, 2011" and "User guide to crystal structure refinement with SHELXL, IUCr, 2008" defined the refinement rules for all H atoms, e.g. positioning with non-idealised geometry using a constrained riding model with C—H distances in the range of 0.70—0.99 Å (AFIX cards were not used) and non-idealised geometry N—H distance in the range of 0.82—0.87 Å (AFIX cards were omitted) (Sheldrick, 2015). The U_{iso}(H) values were set to 1.2 U_{eq} (*C*-aromatic, N) and 1.5 U_{eq} (*C*-methyl), respectively.

Crystal data and conditions of data collection and refinement are reported in Table 1. Data collection for (**I**):

A single crystal was measured on an Eulerian four-circle diffractometer Stoe STADIVARI with a Dectris Pilatus 300 K detector (computing data collection: X-Area Pilatus3_SV 1.31.150.0 (STOE, 2018), computing cell refinement: X-Area Recipe 1.33.0.0 (STOE, 2015), computing data reduction: X-Area Integrate 1.73.1.0 (STOE, 2018), X-Area X-Red32 1.65.0.0 (STOE, 2018), computing publication material: STOE & Cie GmbH, X-Area, software package for collecting single-crystal or multi-domain crystal data on STOE area-detector diffractometers, for image processing, for correction and scaling of reflection intensities and for outlier rejection, version 1.84, (Darmstadt (2018)). Data collection for (**II**): Rigaku Oxford Diffraction, (2022), CrysAlisPro Software system, version 171.42.49 (computing data collection, computing cell refinement and computing data reduction: CrysAlisPro, Agilent Technologies, Version 1.171.37.31), programs used to solve structure

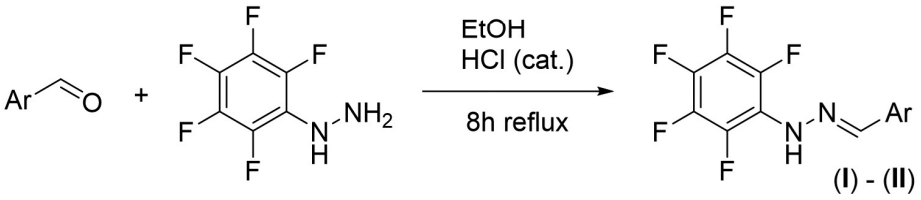

Scheme 3. Ar = 4-bromothiophene-2-yl (**I**), 4-bromo-5-methylthiophene-2-yl (**II**).

(Sheldrick, 2008; Burla et al., 2015), to refine structure (Sheldrick, 2015; Hübschle, 2011), molecular graphics (Brandenburg, 1999), to prepare material for publication (Frisch et al., 2016; Jayatilaka et al., 2005; Spackman et al., 2008; Spackman and Jayatilaka, 2009; Spackman et al., 2021; Sheldrick, 2015; Turner et al., 2017; Dolomanov et al., 2009; Spek, 2003; Hübschle, 2011).

Results and Discussion

The start 'configuration' of the molecules in absolute formulation is known from the synthesis and 'stereochemistry' of atoms in the molecules was confirmed. Molecular geometry and atom numbering scheme of (**I**) and (**II**) are shown in Figs. 1, and 3, respectively. Molecular crystal packing view of (**I**) and (**II**) are shown in Figs. 2 and 4, and experimental characteristics of compounds (**I**) and (**II**) are listed in Table 1, selected geometric parameters are listed in Tables 3 and 5.

Central hydrazone part of the molecule is planar for both title compounds. Atom N1 possesses more negative net charge than N2 (Figs. 5, 6, NBO analysis). Molecular structures are moreover stabilised by one intramolecular N1—H1···F5 hydrogen bond and one intramolecular C12—H12C···Br1 hydrogen interaction only for (**II**) with an H-atom as the donor, Figs. 1, 3, Tabs. 4, 5. The N1—N2 [1. 380 (6)—1. 384 (2) Å] distances are slightly shorter compared to the hydrazine Nsp^2—Nsp^2 (about 1.40 Å) single bond (Allen et al., 1987) and about 1.46 Å single bond (Collin and Lipscomb, 1951) which indicates that there is a significant delocalisation of π-electron density over the hydrazone portion of the molecule. Conformation

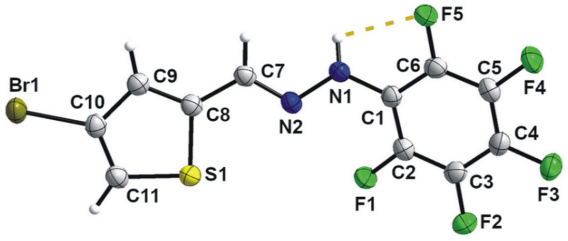

Fig. 1. Molecular structure of title compound (**I**) with atomic numbering scheme. Displacement ellipsoids are drawn at the 50 % probability level.

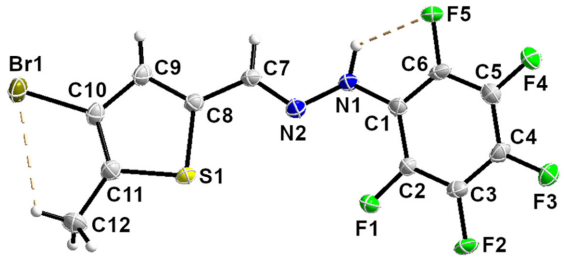

Fig. 3. Molecular structure of title compound (**II**) with atomic numbering scheme. Displacement ellipsoids are drawn at the 50 % probability level.

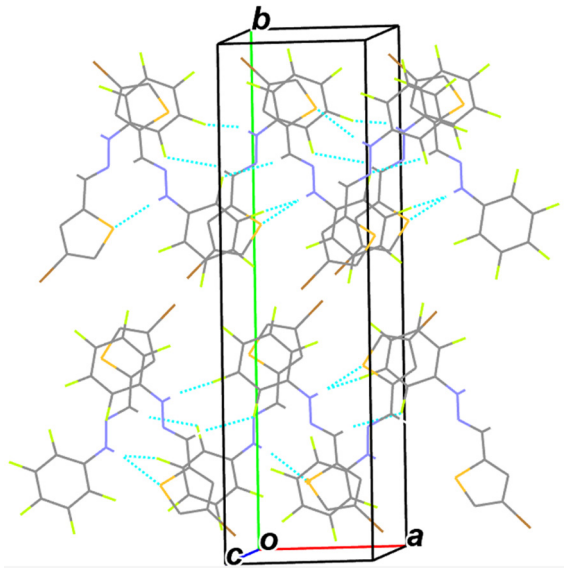

Fig. 2. Part of the crystal structure of title compound (**I**) showing formation of intermolecular hydrogen interactions. Chains of molecular structure of the title compound extend along the *a* axis. H atoms not involved in the motif have been omitted.

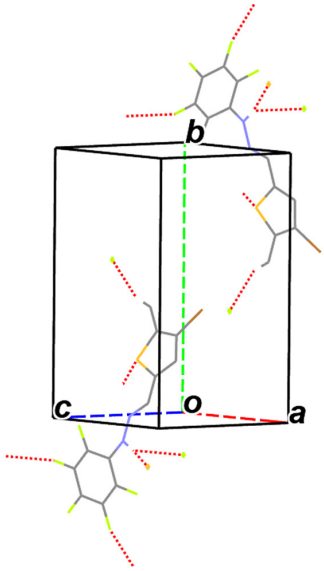

Fig. 4. Part of the crystal structure of title compound (**II**) showing the formation of intermolecular hydrogen interactions. Chains of molecular structure of the title compound extend along the *b* and *c* axes. H atoms not involved in the motif have been omitted.

Tab. 1. Experimental characteristics of compounds (**I**)[a] and (**II**)[b].

Empirical formula	$C_{11}H_4BrF_5N_2S$	$C_{12}H_6BrF_5N_2S$
Formula weight	371.13	385.16
Temperature (K)	298(2)	298(2)
Wavelength (Å)	1.54178	0.71073
Crystal system	Monoclinic	Monoclinic
Space group	$P2_1/n$ (centro)	Pn (non-centro)
Unit-cell dimensions (Å, °)	a = 7.11250(10) b = 25.0194(5) c = 7.1935(2) β = 109.457(2)	a = 7.1916(3) b = 13.5415(5) c = 7.2384(4) β = 109.951(6)
Volume (Å^3)	1206.98(5)	662.61(6)
Z	4	2
Density (calculated) (Mg/m^3)	2.042	1.930
Absorption coefficient (mm^{-1})	6.826	3.311
F(000)	720	376
Crystal size (mm)	0.594 × 0.220 × 0.091	0.591 × 0.306 × 0.065
Theta range for data collection (°)	3.533 to 71.747	1.504 to 32.774
Index ranges	$-8 \le h \le 8$, $-30 \le k \le 29$, $-8 \le l \le 8$	$-10 \le h \le 10$, $-20 \le k \le 20$, $-10 \le l \le 10$
Reflections collected	32397	11109
Independent reflections	2331 [$R_{(int)}$ = 0.0402]	4379 [$R_{(int)}$ = 0.0508]
Completeness to theta (°, %)	67.679, 100.0	25.242, 100.0
Refinement method	Full-matrix least-squares on F^2	Full-matrix least-squares on F^2
Data/restraints/parameters	2331/0/184	4379/2/194
Goodness-of-fit on F^2	1.036	1.032
Final R indices [$I > 2\sigma(I)$]	R_1 = 0.0296, wR_2 = 0.0866	R_1 = 0.0447, wR_2 = 0.1013
R indices (all data)	R_1 = 0.0298, wR_2 = 0.0869	R_1 = 0.0531, wR_2 = 0.1097
Absolute structure parameter	–	0.007(11) (Flack)
Chemical absolute configuration	–	rmad
Extinction coefficient	–	–
Largest diff. peak and hole (e·Å^3)	0.523 and –0.832	1.063 and –1.137

[a]CCDC_2027085,

[b]CCDC_2027086. Crystallographic data for the structures reported in this paper will be available from the Cambridge Crystallographic Data Centre.

Tab. 2. H-bond geometry and Y—X···π-centroid (Cg(1)) stacking interactions (Å, °) for (**I**).

D—H···A	D—H	H···A	D···A Y—X···Cg(1)	D—H···A
N1—H1···F5	0.87(3)	2.39(2)	2.739(2)	105(2)
C7—H7···F1[i]	0.99(3)	2.63(3)	3.404(2)	135(2)
N1—H1···F2[i]	0.87(3)	2.55(3)	3.087(2)	121(2)
N1—H1···S1[ii]	0.87(3)	2.74(3)	3.538(2)	152(2)
C5—F4···Cg(1)[iii]			3.766(2)	

Symmetry codes:
[i] 1 + x, + y, + z;
[ii] 1/2 + x, 1/2 – y, 1/2 + z;
[iii] –1/2 + x, 1/2 – y, –1/2 + z; Cg(1): C8, C9, C10, C11, S1.

Tab. 3. Selected geometric parameters for (**I**): bond lengths (Å), bond and torsion angles (°).

C1—N1	1.393(3)	C7—N2—N1	115.73(17)
C7—N2	1.277(3)	N1—C1—C6—F5	0.8(3)
C8—S1	1.732(2)	N1—C1—C6—C5	–179.68(19)
C9—S1	1.717(2)	N2—C7—C8—C11	174.6(2)
C10—Br1	1.886(2)	N2—C7—C8—S1	–7.3(3)
N1—N2	1.383(2)	S1—C9—C10—C11	–0.2(2)
C7—C8	1.452(3)	S1—C9—C10—Br1	179.47(11)
C2—C1—N1	120.40(18)	Br1—C10—C11—C8	–179.73(15)
N1—C1—C6	123.03(19)	C2—C1—N1—N2	–138.44(19)
N2—C7—C8	119.23(18)	C6—C1—N1—N2	43.9(3)
N2—C7—H7	120.4	C8—C7—N2—N1	176.83(17)
C11—C8—S1	111.53(16)	C1—N1—N2—C7	162.23(18)
C7—C8—S1	120.84(15)	C10—C9—S1—C8	0.33(17)
C10—C9—S1	110.80(16)	C11—C8—S1—C9	–0.34(17)
C9—C10—Br1	123.26(16)	C7—C8—S1—C9	–178.76(17)
C11—C10—Br1	122.38(15)	N1—C1—C2—F1	2.1(3)
N2—N1—C1	117.00(17)	N1—C1—C2—C3	–178.16(18)
C9—S1—C8	91.86(10)		

Tab. 4. H-bond geometry and Y—X···π-centroid (Cg(1)) stacking interactions (Å, °) for (**II**).

D—H···A	D—H	H···A	D···A Y—X···Cg(1)	D—H···A
C12—H12C···Br1	0.99(8)	3.08(8)	3.359(7)	98(5)
N1—H1···F5	0.82(7)	2.28(6)	2.748(5)	117(6)
C12—H12C···Br1^{i}	0.99(8)	3.06(7)	3.892(6)	143(6)
C12—H12B···F4^{ii}	0.95(8)	2.39(8)	3.138(7)	135(6)
N1—H1···F2^{iii}	0.82(7)	2.55(7)	3.084(6)	124(5)
N1—H1···S1^{iv}	0.82(7)	2.91(7)	3.620(5)	146(6)
C2—F1···Cg(1)^{v}			3.924(4)	
C5—F4···Cg(1)^{vi}			3.756(4)	

Symmetry codes:
^{i}x + 1/2, –y + 1, z + 1/2;
^{ii}x, y + 1, z;
^{iii}x, y, z – 1;
^{iv}x – 1/2, –y, z – 1/2;
^{v}–1/2 + x, –y, 1/2 + z;
^{vi}1/2 + x, –y, 1/2 + z;
Cg(1): C8, C9, C10, C11, S1.

of the N1—H1 group of the hydrazone part is advantageous for intramolecular H bond to the hexafluorophenyl part of the molecule(s). Unit-cell density for the parent compound (**I**) is 2.042 g/cm^3 (V = 1206.98, F(000) = 720.0, μ = 6.83 mm^{-1}, cell weight = 1484.53, ρ = 2.042). The introduction of a methyl-substituent to H atom of the thiophene ring for (**II**) changed this to value of 1.930 g/cm^3 (V = 662.61, F(000) = 376.0, μ = 3.31 mm^{-1}, cell weight = 770.32, ρ = 1.930).

Different values of the unit-cell densities indicate the role of the crystallisation process of the substituent on this parameter. The methyl-substituted compound has the lowest value of unit-cell density.

The observed bond lengths and Wiberg bond indices of the compounds showed a clear distinction between single and double bonds in the central spacer unit and the rest of the molecules (Wiberg, 1968). Atoms C7—C8 [1.452 (3) Å, I_w = 1.110 and 1.447, I_w = 1.118] and N2═C7 [1.277 (3) Å, I_w = 1.737 and 1.280, I_w = 1.729] interatomic distances confirm their character as single and double bonds, (Br1—C10: I_w = 1.033 and I_w = 1.027). Atom S1 represents the strong stability effect for this molecule side part (charge 0.433 and 0.425, Figs. 5, 6).

Torsion angle of C2, C1, N1, N2 atoms suggests that H1 atom participates in intra- and intermolecular

Tab. 5. Selected geometric parameters for (**II**): bond lengths (Å), bond and torsion angles (°).

C1—N1	1.390(6)	C7—N2—N1	116.7(4)
C7—N2	1.280(6)	C8—S1—C11	92.8(2)
C7—C8	1.447(7)	N1—C1—C2—C3	179.7(5)
C8—S1	1.725(5)	N1—C1—C6—C5	-177.8(5)
C10—Br1	1.883(5)	N2—C7—C8—C9	173.9(5)
N1—N2	1.380(6)	N2—C7—C8—S1	-8.1(6)
C2—C1—N1	123.4(4)	C12—C11—C10—Br1	3.1(8)
C6—C1—N1	119.8(4)	S1—C11—C10—Br1	-179.7(3)
N2—C7—C8	119.7(4)	Br1—C10—C9—C8	179.8(3)
C9—C8—S1	111.3(4)	C2—C1—N1—N2	44.4(5)
C7—C8—S1	121.5(4)	C6—C1—N1—N2	-138.0(7)
C10—C11—S1	109.1(4)	C8—C7—N2—N1	177.1(4)
C9—C10—Br1	122.9(4)	C1—N1—N2—C7	162.1(4)
C11—C10—Br1	122.1(4)	N2—N1—C1	117.7(4)

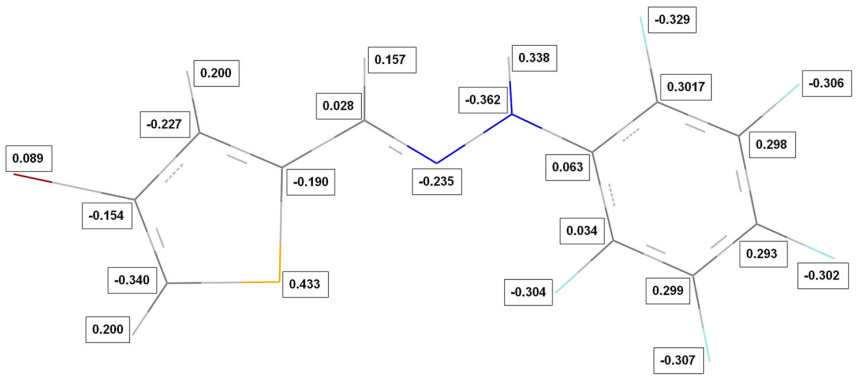

Fig. 5. Molecular structure of title compound (**I**) shoving net atomic charges.

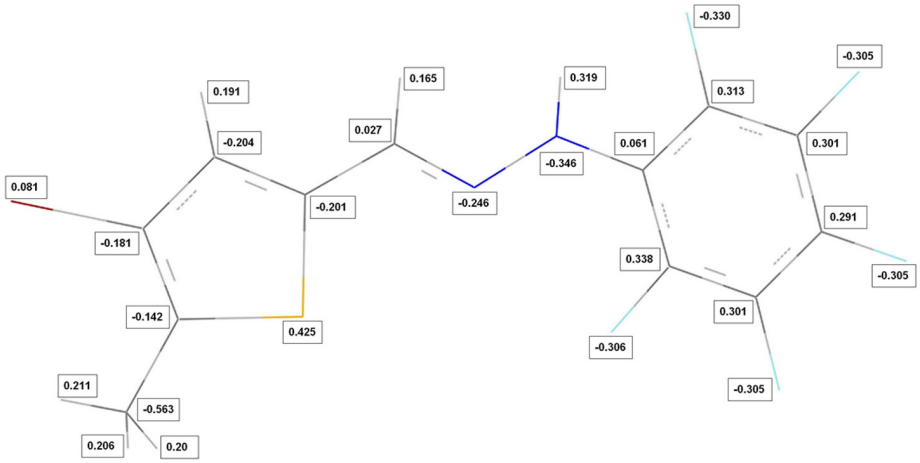

Fig. 6. Molecular structure of title compound (**II**) shoving net atomic charges.

hydrogen bonds. Fig. 7 shows the best least-squares fit (RMS Error = 5.714×10^{-3} Å, atoms C1, N1, N2, C7, C8,) between the close molecules (**I**) and (**II**) (Hypercube, 2007). In Fig. (7) it is shown how molecules fit together to form the molecular structure of (**I**) and (**II**).

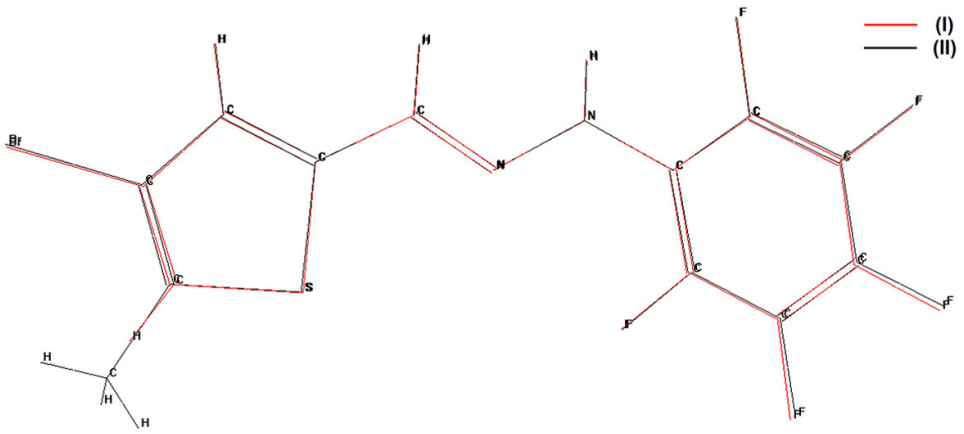

Fig. 7. Molecular structure fit of compounds (**I**) and (**II**).

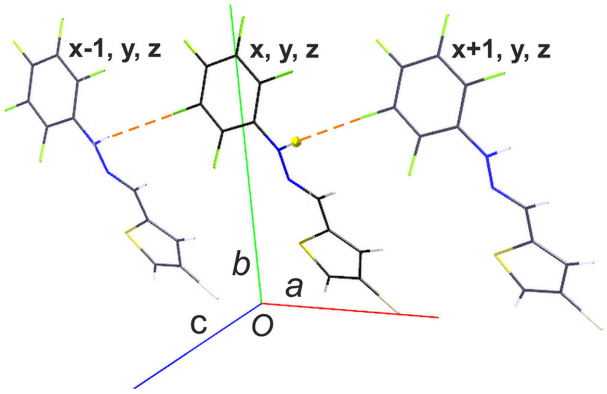

Fig. 8. Molecular packing view of the crystal structure of (**I**) showing the formation of the **C**(6) graph-set motif.

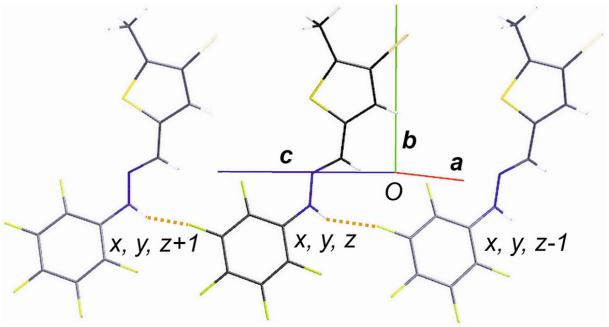

Fig. 9. Molecular packing view of the crystal structure of (**II**) showing the formation of the **C**(6) graph-set motif.

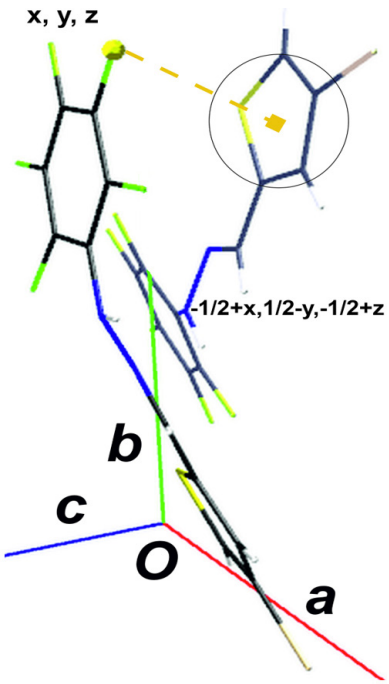

Fig. 10. Molecular packing view of the crystal structure of (**I**) showing the formation of the Y—X···Cg(1) bond motif.

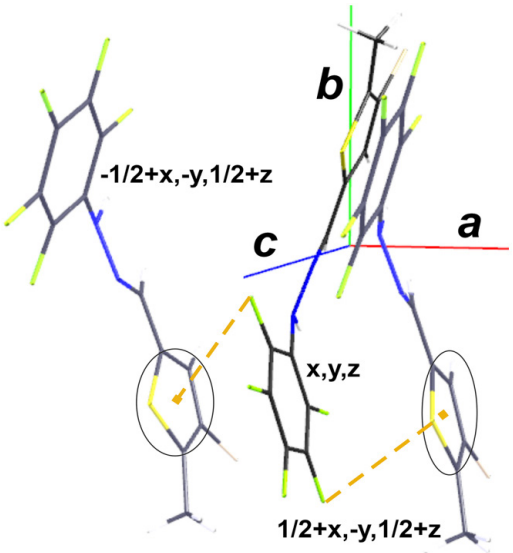

Fig. 11. Molecular packing view of the crystal structure of (**II**) showing the formation of the Y—X···Cg(1) bond motifs.

Graph-set motif of the molecules was proved to be a **C**(6) graph-set motif (Bernstein et al., 1995), (Figs. 8 and 9). Cremer-Pople puckering parameters of the parts of molecules were not confirmed for either crystal structure. Molecular packing view of the crystal structures shows the formation of the Y—X···Cg(1) bond motifs (Figs. 10 and 11).

Results of these calculations are in good agreement with the experimental values of bond lengths found by X-ray structure analysis. NBO analysis of theoretical calculations in vacuum (without an addition of polarisation functions) at the *ab initio* DFT/B3LYP level using the 6-311G basis set model (single point geometry, NBO net charges) is shown for selected atoms in Figs. 5 and 6. Hirshfeld surface analysis is a powerful tool for gaining additional view into the intermolecular interactions of molecular crystals. The size, shape and type of Hirshfeld surface allows for qualitative and quantitative investigation and visualisation of intermolecular close contacts in molecular crystals. The structure with its Hirshfeld's approach considers each molecule enclosed surface (Hirshfeld surface) so that in any point, half or more electron density comes from the atoms of the molecule. The Hirshfeld surface map over d_{norm} analyses the electron density, shape-index, and the curvedness of a surface. Hirshfeld surface (Figs. 12 and 13) shows simple workable places for biological activity including the shortest distances of worthy molecule-hydrogen bonds to suitable receptor site-locality and thus for the molecular "dimension", biological activities will be as few as adequate (d_{norm} range of (–0.187, 1.017) and d_{norm} range of (–0.193, 1.116), atoms within the radius of 3.80 Å). Hirshfeld surface analysis was carried out in order to study the nature of the surface molecu-

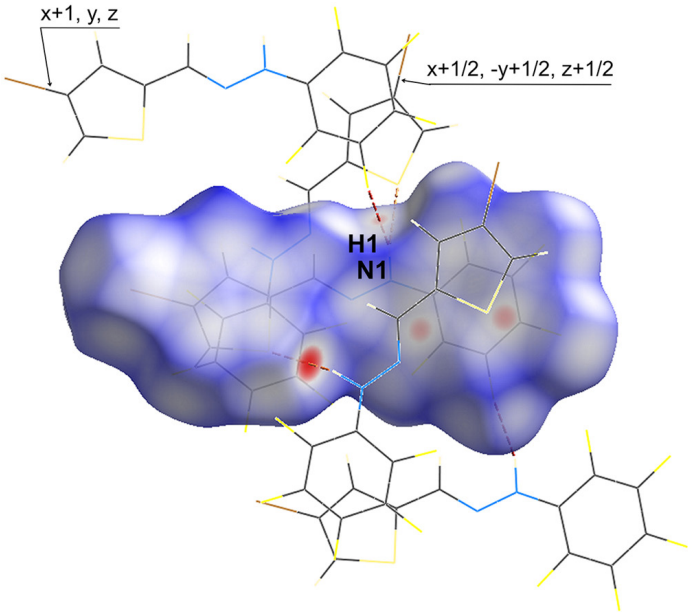

Fig. 12. Simple Hirshfeld surface for title compound (**I**).

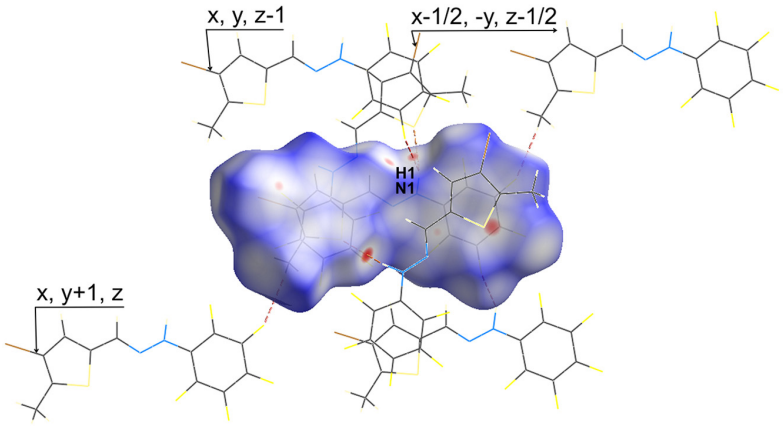

Fig. 13. Simple Hirshfeld surface for title compound (**II**).

Tab. 6. Interaction energies (kJ/mol, kcal/mol) for (**I**).

R	E_ele	E_pol	E_dis	E_rep	E_tot	complexation energy (raw)/ (corrected)
C7—H7···F1, N1—H1···F2, 1 + x, + y, + z						
7.11	–6.91	–1.79	–23.38	11.70	–21.76	–10.82/–6.00
N1—H1···S1, 1/2 + x, 1/2 – y, 1/2 + z						
4.23	–17.23	–3.81	–58.08	52.65	–39.09	–15.82/–11.15
C5—F4···Cg(1), –1/2 + x, 1/2 – y, –1/2 + z						
4.23	–17.23	–3.81	–58.08	52.65	–39.09	–15.82/–11.15

Tab. 7. Interaction energies (kJ/mol, kcal/mol) for (**II**).

R	E_ele	E_pol	E_dis	E_rep	E_tot	complexation energy (raw)/ (corrected)
C12—H12C···Br1, x + 1/2, –y + 1, z + 1/2						
13.08	–1.13	–0.37	–7.50	0.00	–8.00	–3.61/–1.72
C12—H12B···F4, + x, + y + 1, + z						
13.54	–0.56	–0.26	–6.26	0.00	–6.23	–2.91/–1.61
N1—H1···F2, + x, + y, + z – 1						
7.24	–7.07	–1.68	–25.61	13.95	–22.40	–11.66/–6.30
N1—H1···S1, x – 1/2, –y, z – 1/2						
4.29	–17.31	–3.31	–60.91	49.97	–42.92	–17.01/–12.10
C2—F1···Cg(1), –1/2 + x, –y, 1/2 + z						
6.02	–10.82	–1.12	–45.72	32.09	–32.26	–13.93/–6.50
C5—F4···Cg(1), 1/2 + x, –y, 1/2 + z						
4.29	–17.31	–3.31	–60.91	49.97	–42.92	–17.01/–12.10

lar bond contacts of the title compounds. Hirshfeld surfaces were generated using CrystalExplorer 17.5 to analyse the nature of the intermolecular contacts and their quantitative contributions to the crystal packing in (**I**) and (**II**). Electrostatic potentials, obtained using TONTO, integrated in CrystalExplorer using the DFT/B3LYP/6-31G basis set model were involved to map the Hirshfeld surfaces over the electrostatic potentials.

To define CrystalExplorer model energies, total energy of interaction between molecules in the crystal structure is commonly expressed in terms of four key components: electrostatic, polarisation, dispersion, and exchange-repulsion and the preferred energy model B3LYP/6-31G(d, p) was employed. The model B3LYP/6-31G(d,p) 6d 10f NoSymm Counterpoise=2 EmpiricalDispersion=GD2 was applied by Gaussian.

The CrystalExplorer and Gaussian unit cell crystal packing model energies for (**I**) and (**II**) are listed in Tables 6 and 7, respectively. It is noteworthy that binding abilities with N1—H1···S1 hydrogen bond geometry and corrected complexation energy results are more effective in (**I**) compared to (**II**) considering the same participation of N1—H1···S1 with respect to the appropriate crystal structure.

Conclusions

1-((4-Bromothiophen-2-yl)methylene)-2-(perfluorophenyl)hydrazine and 1-((4-bromo-5-methylthiophen-2-yl) methylene)-2-(perfluorophenyl)hydrazine were synthesised and NMR spectra, X-ray investigation, and Gaussian analyses were performed. Two hydrazone derivatives and its "chemical, molecular-structural, NBO charges, Hirshfeld surface and fitting interaction properties" were confirmed experimentally as well as theoretically. Atoms of sulfur, nitrogen and their hydrogen atoms play a considerable role in the bond system of the molecule and participate in the "configuration diversity" of the spatial forms of the molecules in the crystal structure. "Conformation diversity" has not been shown in the fitting scheme (Fig. 7).

Acknowledgement

This contribution was written thanks to the generous support under the Operational Program Integrated Infrastructure for the project: "Strategic research in the field of SMART monitoring, treatment and preventive protection against coronavirus (SARS-CoV-2)", Project no. 313011ASS8, co-financed by the European Regional Development and the Fund Science and Technology Assistance Agency under contract No. APVV-17-0513 and APVV-20-0213.

References

Allen FH, Kennard O, Watson DG, Brammer L, Orpen AG, Taylor R (1987) J. of the Chemical Society, Perkin Transactions 2: 12 S19.

Baier A, Kokel A, Horton W, Gizińska E, Pandey G, Szyszka R, Török B, Török M (2021) ChemMedChem Agric.FoodChem. 16: 1927—1932.

Bari A, Grenier D, Azelmat J, Syed SA, Al-Obaid AM, Hosten EC (2019) Chem. Biol. Drug Des. 94 4: 1750—1759.

Bernstein J, Davis RE, Shimoni L, Chang NL (1995) Angew. Chem. Int Ed. Engl. 34: 1555—1573.

Beverina L, Drees M, Facchetti A, Salamone M, Ruffo R, Pagani GA (2011) Eur. J. Org. Chem. 28: 5555—5563.

Bortňák D, Pecher D, Végh D, Breza M, Mikuš P, Milata V (2020) J. of Mass Spectrometry 55(10): e4540.

Brandenburg K (1999) Crystal Impact GbR Bonn Germany.

Burdette SC (2012) Nat. Chem. 4 (9): 695—699.

Burla MC, Caliandro R, Carrozzini B, Cascarano GL, Cuocci C, Giacovazzo C, Mallamo M, Mazzone A, Polidori G (2015) J. Appl. Cryst. 48: 306—309.

Collin RL, Lipscomb WN (1951) Acta Cryst. 4: 10—14.

Dolomanov OV, Bourhis LJ, Gildea RJ, Howard JAK, Puschmann H (2009) J Appl. Cryst. 42: 339—341.

Eloh K, Demurtas M, Deplano A, Mfopa AN, Murgia A, Maxia A, Onnis V, Caboni P (2015) J. Agric. Food Chem. 63(45): 9970—9976.

Feringa BL, Browne WR (2011) Molecular Switches Vol. I, II 595—627; Feringa BL, Browne WR Eds.; Wiley-VCH Verlag GmbH & Co. KGaA Weinheim.

Frisch MJ, Trucks GW, Schlegel HB, Scuseria GE, Robb MA, Cheeseman JR, Scalmani G, Barone V, Petersson GA, Nakatsuji H, Li X, Caricato M, Marenich AV, Bloino J, Janesko BG, Gomperts R, Mennucci B, Hratchian HP, Ortiz JV, Izmaylov AF, Sonnenberg JL, Williams-Young D, Ding F, Lipparini F, Egidi F, Goings J, Peng B, Petrone A, Henderson T, Ranasinghe D, Zakrzewski VG, Gao J, Rega N, Zheng G, Liang W, Hada M, Ehara M, Toyota K, Fukuda R, Hasegawa J, Ishida M, Nakajima T, Honda Y, Kitao O, Nakai H, Vreven T, Throssell K, Montgomery JA Jr, Peralta JE, Ogliaro F, Bearpark MJ, Heyd JJ, Brothers EN, Kudin KN, Staroverov VN, Keith TA, Kobayashi R, Normand J, Raghavachari K, Rendell AP, Burant JC, Iyengar SS, Tomasi J, Cossi M, Millam JM, Klene M, Adamo C, Cammi R, Ochterski JW, Martin RL, Morokuma K, Farkas O, Foresman JB, Fox DJ (2016) Gaussian 16 Revision D.01 Gaussian Inc. Wallingford CT.

Giliberti G, Ibba C, Marongiu E, Loddo R, Tonelli M, Boido V, Laurini E, Posocco P, Fermeglia M, Pricl S (2010) Bioorganic Med. Chem. 18(16): 6055—6066.

Ghosh P, Hazra A, Ghosh M, Chandra Murmu N, Banerjee P (2018) J. Mol. Struct. 1157: 444—449.

Hübschle ChB, Sheldrick GM, Dittrich B (2011) J App. Cryst. 44: 1281—1284.

Hypercube Inc. (2007) Hyperchem 7.0 Gainesville FL 32601 USA.

Chowdhury AR, Ghosh P, Roy BG, Mukhopadhyay SK, Murmu NC, Banerjee P (2015) Aqueous Solvent. Sensors Actuators B. Chem. 220: 347—355.

Jayatilaka D, Grimwood DJ, Lee A, Lemay A, Russel AJ, Taylor C, Wolff SK, Cassam-Chenai P, Whitton A (2005) TONTO.

Kuman L, Chauhan LJ (2014) Chem. Pharm. Res. 6(12): 916.

Lukeš V, Michalík M, Poliak P, Cagardová D, Végh D, Bortňák D, Fronc M, Kožíšek J (2016) Terminal Unit. Synth. Met. 219: 83—92.

Oxford Diffraction (2012) CrysAlis CCD and CrysAlis RED Oxford Diffraction Ltd, Yarnton, Oxfordshire, England.

Saha SJ, Siddiqui AA, Pramanik S, Saha D, De R, Mazumder S, Debsharma S, Nag S, Banerjee C, Bandyopadhyay U (2019) ACS Infect. Dis., 5(1): 63—73.

Sandoval-Torrientes R, Pascual J, García-Benito I, Collavini S, Kosta I, Tena-Zaera R, Martín N, Delgado JL (2017) ChemSusChem 10(9): 2023—2029.

Sheldrick GM (2008) SHELXS Acta Cryst. A64: 112—122.

Sheldrick GM (2015) SHELXL Acta Cryst. C71: 2053—2096.

Spackman MA, Jayatilaka D (2009) CrystEngComm 1: 19—32 Chemistry M313 School of Biomedical Biomolecular and Chemical Sciences University of Western Australia.

Spackman MA, McKinnon JJ, Jayatilaka D (2008) CrystEngComm. 10: 377—388.

Spackman PR, Turner MJ, McKinnon JJ, Wolff SK, Grimwood DJ, Jayatilaka D, Spackman MA (2021) Crystal Explorer 21.5 University of Western Australia Perth Australia.

Spek AL (2003) J Appl. Cryst. 36: 7—13.

STOE & Cie GmbH (2018) X-AREA Stoe & Cie GmbH, Darmstadt, Germany.

Su X, Aprahamian I (2014) Chemical Society Reviews March 21: 1963—1981.

Tarabová D, Milata V (2012) Acta Chimica Slovaca 5 2: 232—235.

Tonelli M, Boido V, Canu C, Sparatore A, Sparatore, F, Paneni MS, Fermeglia M, Pricl S, La Colla P, Casula L, Ibba C, Collu D, Loddo R (2008) Bioorganic Med. Chem. 16 (18): 8447—8465.

Turner MJ, McKinnon JJ, Wolff SK, Grimwood DJ, Spackman PR, Jayatilaka D, Spackman MA (2017) CrystalExplorer 17.5 University of Western Australia.

Verma G, Marella A, Shaquiquzzaman M, Akhtar M, Ali MR, Alam MM (2014) J. of Pharmacy and Bioallied Sciences 69—80.

Wiberg KB (1968) Tetrahedron 24: 3 1083—1096.

Xu W, Shao Z, Han Y, Wang W, Song Y, Hou H (2018) Elsevier Ltd. 152: 171—179.